Requirement and Synergistic Contribution of Platelet-Activating Factor Acetylhydrolase Sse and Streptolysin S to Inhibition of Neutrophil Recruitment and Systemic Infection by Hypervirulent emm3 Group A Streptococcus in Subcutaneous Infection of Mice

Authors: Wenchao Feng, Dylan Minor, Mengyao Liu, & Benfang Lei

Requirement and Synergistic Contribution of PAF acetylhydrolase Sse and Streptolysin S to Inhibition of Neutrophil Recruitment and Systemic Infection by Hypervirulent *emm*3 Group A *Streptococcus* in Subcutaneous Infection of Mice

Wenchao Feng, Dylan Minor, Mengyao Liu, and Benfang Lei*

Department of Microbiology and Immunology, Montana State University, Bozeman, MT 59718

Running Title: Synergistic Effects of Sse and SLS on GAS Immune Evasion

*Correspondence to Benfang Lei, blei@montana.edu

(ABSTRACT)

Hypervirulent Group A Streptococcus (GAS) can inhibit neutrophil recruitment and cause systemic infection in mouse model of skin infection. The purpose of this study was to determine whether PAF acetylhydrolase Sse and streptolysin S (SLS) have synergistic contributions to inhibition of neutrophil recruitment and systemic infection in subcutaneous infection of mice by MGAS315, a hypervirulent genotype *emm*3 GAS strain. Deletions of *sse* and *sagA* in MGAS315 synergistically reduced skin lesion size and GAS burden in the liver and spleen. However, the mutants were persistent at skin sites and had similar growth factors in nonimmune blood. Thus, the low Δ*sse*Δ*sagA* numbers in the liver/spleen is likely due to its reduction in systemic dissemination. Few intact and necrotic neutrophils were detected at MGAS315 infection sites. In contrast, many neutrophils and necrotic cells were present at the edge of Δ*sse* sites on day 1 and at the edge and inside of Δ*sse* sites on day 2. Δ*sagA* sites had massive and few intact neutrophils at the edge and center of infection sites, respectively, on day 1 and were full of intact neutrophils or necrotic cells on Day 2. Δ*sse*Δ*sagA* sites had massive intact neutrophils in the whole infection sites. These *sse* and *sagA* deletion-caused changes in the histological pattern at skin infection sites can be complemented. Thus, *sse* and *sagA* deletions synergistically enhance neutrophil recruitment. These findings indicate that Sse and SLS are both required but neither is sufficient for inhibition of neutrophil recruitment and systemic infection by hypervirulent GAS.

(INTRODUCTION)

Group A streptococcus (GAS) is a major human pathogen that commonly causes relatively mild pharyngitis and superficial skin infections (1). GAS can also cause potentially lethal severe invasive infections with about 12,000 cases annually in the United States, and these severe infections include bacteremic skin and soft-tissue infections, pneumonia, necrotizing fasciitis, and bacteremia without focus (2). The severe invasive infections in 2005 to 2012 in the United States are most frequently associated with GAS of the M protein gene-based genotypes *emm*1, *emm*12, *emm*3, *emm*28, and *emm*89 (2). Invasive *emm*3 GAS causes a higher mortality rate than invasive strains of other serotypes (3).

Necrotizing fasciitis (NF) is a rapidly progressive infection of the skin, subcutaneous and deep soft tissue, and muscle and leads to systemic dissemination (4). Some NF patients have numerous bacteria but few or no neutrophilic responses at infection sites (5, 6), which is classified as stage III NF (6), and other histopathologic types include a moderate-to-severe neutrophilic response (stage II) and positive Gram stain and an intense neutrophilic response and an absence of bacteria (stage I) in infected tissues (6). Patients with the stage III NF have higher mortality rate than patients with stages I and II NF (5, 6).

Murine NF model with hypervirulent, invasive M1T1 GAS displays the stage III histopathologic features, few or no neutrophils at bacterial sites (7, 8). Hypervirulent M1T1 GAS isolates are usually natural CovRS mutants (8-10). CovRS (also known as CsrRS) is the two-component regulatory system that negatively regulates multiple virulence factors (11-14), including those involved in innate immune evasion, such as the capsule synthase HasA (11), IL-8/CXC chemokine peptidase SpyCEP (15), platelet-activating factor acetylhydrolase SsE (7, 16), opsonophagocytosis-inhibiting Mac (17), NAD^+-glycohydrolase (18), and streptolysin O (19). Natural CovRS mutations of a M1T1 clone of serotype M1 GAS enhance the expression of

CovRS-controlled virulence factors and down-regulates the expression of the protease SpeB, resulting in a high capacity to cause skin invasion, innate immune evasion, systemic dissemination, and hypervirulence (8, 14, 20, 21). The selection of CovRS M1T1 mutations during infection has been readily demonstrated in invasive M1T1 GAS during experimental mouse infections (10, 20-26). Neutrophils are required for *in vivo* selection of *covRS* mutants, and M1T1 CovRS mutants exhibit greater resistance to clearance by neutrophils *in vivo* (27).

The severe inhibition of neutrophil responses by M1T1 GAS requires CovRS mutations, and the PAF acetylhydrolase Sse, but not IL-8 peptidase SpyCEP and C5a peptidase ScpA, plays a critical role in inhibition of neutrophil recruitment by hypervirulent M1T1 GAS CovS mutants (7, 8). Streptolysin S (SLS) has been shown to inhibit neutrophil recruitment in a zebrafish model of GAS infection and delays the exodus of the neutrophils from the vessel lumen into the tissue at the early stage of GAS skin infection in mice (28). The purpose of this manuscript was to determine whether Sse and SLS have synergistic effect on the capacity of MGAS315, a hypervirulent *emm*3 strain (29, 30), to inhibit neutrophil recruitment and to cause systemic infection in subcutaneous infection of mice. We generated single and double deletion mutants of MGAS315 for *sagA*, which encodes the peptide component of SLS, and *sse*. We found that *sse* and *sagA* deletions synergistically reduce skin invasion and GAS load in the liver and spleen and that both *sse* and *sagA* are both required for inhibition of neutrophil recruitment by MGAS315.

RESULTS

Synergistic effects of Sse and SLS to skin invasion, systemic infection, and neutrophil recruitment in murine model of subcutaneous MGAS315 infection. MGAS315 caused large lesions in female CD-1 mice at 48 h after subcutaneous inoculation (Lesion area ± SD: 934 ± 165 mm^2) whereas MGAS315 Δ*sse*, Δ*sagA*, and Δ*sse*Δ*sagA* caused lesion sizes of 277

82 ± 64, 380 ± 126, and 188 ± 58 mm^2, respectively (Fig. 1A and 1B). There were (4.0 ± 2.6) x 10^4
83 neutrophils at the MGAS315 skin infection site as estimated by the myeloperoxidase (MPO)
84 assay, and Δ*sse*, Δ*sagA*, and Δ*sse*Δ*sagA* recruited (2.8 + 1.5) x 10^5, (2.5 + 0.8) x 10^5, and (5.1 +
85 1.3) x 10^5 neutrophils at the infection sites, respectively. There were (2.5 + 3.6) x 10^8 and 2.0 +
86 1.1 x 10^7 GAS bacteria in the spleen and in per gram liver tissue in the MGAS315 infection,
87 respectively, and deletion of *sse* or *sagA* in MGAS315 reduced GAS loads in the spleen by the
88 magnitude of ≥4 orders and in the liver by the magnitude of 2 orders (Fig. 1). More importantly,
89 there were no GAS in the liver and spleen of the majority of mice infected with Δ*sse*Δ*sagA* on
90 day 2 after inoculation (Fig. 1C and 1D). The data indicate that Sse and SLS significantly
91 contribute to skin invasion, inhibition of neutrophil recruitment, and systemic infection in
92 subcutaneous infection of mice and that Sse and SLS have synergistic contribution to skin
93 invasion, inhibition of neutrophil recruitment, and systemic infection in skin infections of CD-1
94 mice.

95 These strains were also compared in subcutaneous infection of C57BL/6J mice on day 1
96 after inoculation. The effects of *sse* and/or *sagA* deletions in MGAS315 on skin invasion,
97 neutrophil recruitment, and bacterial loads in the liver and spleen in C57BL/6J mice were similar
98 to those in CD-1 mice (Fig. 2). Particularly, the *sse* and *sagA* deletions also showed the
99 synergistic contribution to the enhancement in neutrophil recruitment and reduction in GAS
100 loads in the liver and spleen. We also compared Δ*sse* infection in female and male C57BL/6J
101 mice and observed no gender difference in lesion size, neutrophil levels, and GAS loads in the
102 liver and spleen (Fig. 2).

103 **Resistance of MGAS315 and its *sse* and *sagA* deletion mutants to clearance at skin**
104 **infection sites and in nonimmune human and mouse blood.** Bacterial loads of Δ*sse*Δ*sagA* in

the liver and spleen at days 1 and 2 after inoculation were >1000-fold lower than those of MGAS315, Δ*sse*, and Δ*sagA*. This difference could be due to effective clearance of Δ*sse*Δ*sagA* at skin infection sites because of the more robust neutrophil recruitment at Δ*sse*Δ*sagA* sites. Alternatively, the double mutant might be compromised in growth and survival in blood. These possibilities were examined. The numbers of viable GAS at skin infection sites at 24 h after inoculation were 286%, 156%, 55%, and 85% of those at 1 h after inoculation in MGAS315, Δ*sse*, Δ*sagA*, and Δ*sse*Δ*sagA* infections, respectively (Fig. 3A). The numbers of wt strain and Δ*sse* at skin infection sites slightly increased whereas the numbers of Δ*sagA* and Δ*sse*Δ*sagA* slightly decreased with time. The data indicate that the mutants with enhanced neutrophil responses, especially Δ*sse*Δ*sagA,* were not efficiently cleared at 24 h after inoculation. To determine whether the mutants were compromised in growth and survival in blood, the apparent growth factors of MGAS315 and its Δ*sse*, Δ*sagA*, Δ*sse*Δ*sagA* mutants, and their complement strains in heparinized blood and serum from two persons and in pooled heparinized mouse blood were measured. The two persons were healthy and lacked anti-SLO and anti-NADase antibodies in their serum (data not shown). The numbers of MGAS315, the mutants, and complement strains of the mutants after 3-h incubation in blood and sera were more than 40-fold higher than inoculum (Fig. 3B). The apparent growth factors of the test strains in each test had no significant difference as the 1 way ANOVA multiple comparison analyses of the data using the GraphPad Prism software (version 7.03) resulted in P values of ≥0.1184. Thus, the *sse* and/or *sagA* deletions did not alter growth and survival of MGAS315 in human and mouse blood. These data suggest that the lowered loads of the *sse* and *sagA* deletion mutants in the liver and spleen appears to at least partially be due to reduced systemic dissemination.

Inhibition of neutrophil recruitment inside skin infection sites by MGAS315. The MPO assay data in Figs. 1 and 2 indicate that there was no robust neutrophil response at MGAS315 infection sites in the skin. The Gram and H&E stain patterns were consistent with this measurement. Presentative Gram and H&E stain images of a section covering the center of the whole subcutaneous infection site at days 1 and 2 after GAS inoculation are shown in Figs. S1 and S2, respectively. Bacterial sites are referred as GAS zone, and a thin layer of neutrophils referred as neutrophil zone was present at the edge of GAS zone. Images at higher magnification show that bacterial site had very few neutrophils or necrotic materials, which is indicated by the dashed, red box on both days 1 and 2 after inoculation of MGAS315 (Figs. 4 and 5). There was a thin layer of neutrophils on day 1 and more neutrophils on day 2, which are indicated by the dashed, yellow box. The yellow box of the neutrophil zone was at the edge of the GAS site, and the red and yellow boxes were not overlapped with each other. These results indicate that MGAS315 can inhibit neutrophil recruitment within GAS sites.

Synergistic effect of *sse* and *sagA* deletions on neutrophil recruitment inside GAS sites. Skin infection sites were analyzed by Gram and H&E stains for subcutaneous infections of C57BL/6J mice with Δ*sse*, Δ*sagA*, and Δ*sse*Δ*sagA* at 24 h (5 mice) and 48 h (5 mice) after inoculation. A series of sections through each skin infection site were analyzed by Gram and H&E stains, and representative stain images of whole skin infection sites at days 1 and 2 are presented as Figs. S3-S8. The stain patterns of Δ*sse* site at day 1 (Fig. S3) was largely similar to that of MGAS315 site (Fig. S1), having neutrophils mainly at the edge of bacterial sites. However, the higher magnification images show a couple of differences between MGAS315 and Δ*sse* sites. More neutrophils were present at the edge of Δ*sse* site and were engaged with bacteria (pink box), and an intense stain zone of bacteria and necrotic materials (green box) was

between the intense neutrophil/GAS zone (pink box) and sites with free bacteria and few neutrophils (red box) (Fig. 4). While the stain patterns of MGAS315 site on day 2 were very similar to that of MGAS315 site on day 1, the stain patterns of Δ*sse* site on day2 were totally different from those of Δ*sse* site on day 1 and MGAS315 site on day 2, showing robust neutrophil recruitment throughout the whole infection site (Fig. S4). The higher magnification images of Δ*sse* site on day 2 in Fig. 5 show intense staining of bacteria and necrotic neutrophils (green box) and staining of intact neutrophils and bacteria at the edges of infection site (yellow box). Thus, deletion of *sse* abolishes MGAS315 inhibition of neutrophil recruitment inside GAS site.

The deletion of *sagA* had more profound effect on neutrophil recruitment than *sse* deletion on day 1 (Fig. S5). Δ*sagA* site on day 1 showed intense neutrophil stains at the edge (pink box), and free bacteria and fewer neutrophils were observed at the center of Δ*sagA* sites , which contained bacteria/necrotic material regions (green box), and region containing mainly free bacteria (red box) (Fig. 4). Compared with Δ*sse* site, Δ*sagA* site on day 2 showed more intense staining of intact neutrophils (pink box) and had necrotic materials only at the center of infection site (green box) (Figs. 5 and S6). Thus, deletion of *sagA* also abolishes MGAS315 inhibition of neutrophil recruitment inside GAS site.

In contrast to the Δ*sse* and Δ*sagA* infection in which the center of Δ*sse* and Δ*sagA* sites had sparsely scattered neutrophils at day 1 after inoculation, Δ*sse*Δ*sagA* site was almost full of neutrophils at day 1 after inoculation (Figs. 4 and S7). Stain patterns of Δ*sse*Δ*sagA* on day 2 were similar to those on day 1 (Figs. 5 and S8). These results indicate that the *sse* and *sagA* deletions have synergistic promotion of neutrophil recruitment inside GAS sites in the skin.

Thus, neither of Sse or SLS is sufficient to cause the inhibition of neutrophil infiltration by MGAS315, and both Sse and SLS are required for and synergistically contribute to inhibition of neutrophil recruitment by MGAS315. In addition, Δ*sse*Δ*sagA* sites on both days did not have many necrotic neutrophils, suggesting that Sse and SLS can both contribute to apoptosis or necrosis of recruited neutrophils.

Complementation of Δ*sse, ΔsagA,* and Δ*sse*Δ*sagA*. To confirm the phenotype of Δ*sse*, Δ*sagA*, and Δ*sse*Δ*sagA* was due to the *sse* and *sagA* deletions but not a spurious mutation, the *sse* gene was put back into Δ*sse* and Δ*sse*Δ*sagA*, and the *sagA* gene was put back to Δ*sagA* and Δ*sse*Δ*sagA*, yielding Δ*sse-sse*, Δ*sagA-sagA*, Δ*sse*Δ*sagA-sse* and Δ*sse*Δ*sagA-sagA*. These complementation strains of the *sse* and *sagA* deletion mutants restored Sse production and SLS, respectively, according to the PAF acetylhydrolase activity in the culture supernatant of Δ*sse-sse* and Δ*sse*Δ*sagA-sse* and β-hemolytic activity of Δ*sagA-sagA* and Δ*sse*Δ*sagA-sagA* on blood agar plates (data not shown). The histological patterns of these complementation strains in subcutaneous infection of C57BL/6J mice were determined on days 1 and 2 after inoculation. The Gram and H&E stain pattern of Δ*sse-sse* (Fig. S9) and Δ*sagA-sagA* (Fig. S10) were similar to that of MGAS315 (Figs. S1 and S2), and the pattern of Δ*sse*Δ*sagA-sse* (Fig. S11) and Δ*sse*Δ*sagA-sagA* (Fig. S12) were similar to that of Δ*sagA* (Figs. S5 and S6) and Δ*sse* (Figs. S3 and S4), respectively. In addition, the levels of *emm*3, *hasA*, *spyCEP*, and *scpA* transcripts in Δ*sse*, Δ*sagA*, Δ*sse*Δ*sagA* at the exponential growth phase in THY were similar to those of MGAS315 (data not shown). Thus, the phenotype of Δ*sse*, Δ*sagA*, and Δ*sse*Δ*sagA* is caused by the *sse* and/or *sagA* deletions.

For better understanding of the histopathological features of the skin infections in the histological figures, Gram and H&E stain images of the skin of C57BL/6J without GAS infection is presented in Fig. S13 for comparison.

DISCUSSION

This study was designed to examine the role of Sse and SLS in the inhibition of neutrophil recruitment by hypervirulent *emm*3 GAS. The findings are as follows: 1) deletion of *sse* or *sagA* enhances neutrophil recruitment and reduces skin invasion and GAS loads in the liver and spleen in subcutaneous infection of mice with MGAS315; 2) MGAS315 inhibits neutrophil recruitment inside GAS sites, and both *sse* and *sagA* are required for the inhibition of neutrophil recruitment; and 3) *sse* and *sagA* deletions have synergistic effects on skin invasion, neutrophil recruitment, and systemic infection. These findings indicate that Sse and SLS are required but either of them is not sufficient for the inhibition of neutrophil recruitment by hypervirulent *emm*3 GAS and synergistically contribute to GAS skin invasion and systemic GAS infections.

Bakleh *et al*. has classified necrotizing fasciitis caused by GAS into 3 stages according to histopathologic features (6). Stage I NF has intense neutrophilic response and an absence of bacteria in Gram stain; stage II NF has a moderate-to-severe neutrophilic response and positive Gram stain; and stage III NF is characterized by the presence of few or no neutrophils and a Gram stain results positive for bacteria. Patients with stage III NF have a higher mortality rate than patients with stage I and II NF. The subcutaneous MGAS315 infection site in mice displays the stage III histopathologic features. Skin infection sites of MGAS5005 in mice also have few

neutrophils at sites where Gram stain is positive for GAS (7). MGAS5005, a M1T1 isolate, and MGAS315 are both hypervirulent CovS mutants, and the correction of their *covS* mutation enhances neutrophil recruitment by more than 10 fold (8, 30). Thus, the findings in our current and previous studies indicate that hypervirulent M1T1 and M3 GAS CovRS mutants can cause the stage III histopathologic pattern in skin infections by inhibiting neutrophil recruitment.

The enhancement in neutrophil recruitment by *sse* deletion in MGAS315 confirms our previous findings on the function of Sse in inhibition of neutrophil responses. Deletion of *sse* in M1T1 strain MGAS5005 enhances neutrophil recruitment (7). Sse is a potent PAF acetylhydrolase, and the function of Sse is medicated by targeting PAF (7, 31). Passive immunization with an enzymatic activity-neutralizing monoclonal antibody of Sse enhances neutrophil recruitment (32). Sse, but not CXC chemokine peptidase SpyCEP and C5a peptidase ScpA, is critical for MGAS5005 inhibition of neutrophil recruitment in skin infection of mice (8). Our results indicate that Sse also plays a critical role in the inhibition of neutrophil recruitment by hypervirulent *emm*3 GAS.

SLS is another critical factor for the inhibition of neutrophil responses by MGAS315 in skin infection of mice. SLS is a cytolytic toxin, and its peptide component is encoded by *sagA* (33). GAS *sagA* deletion mutant is attenuated in virulence and skin invasion (34). SLS-negative mutant is associated with the robust recruitment of neutrophils and significantly reduces lethal myositis in zebrafish, and the extravasation of neutrophils is quicker in the early stage of subcutaneous infection of mice with SLS^- mutant than wild-type GAS (28). In this study, we show that SLS is required for the inhibition of neutrophil recruitment by hypervirulent M3 GAS. Thus, both *sse* and *sagA* are essential but not sufficient for the inhibition of neutrophil recruitment by hypervirulent M3 GAS CovS mutants in subcutaneous infections of mice.

238 The essential but insufficient role of each of Sse and SLS in MGAS315 inhibition of
239 neutrophil recruitment implies that Sse and SLS evade neutrophil responses through different
240 mechanisms. The synergistic effects of *sse* and *sagA* deletions on neutrophil recruitment support
241 this implication. Sse has the potent PAF acetylhydrolase activity, and neutrophil recruitment is
242 lowered in infection of PAF receptor KO mice with MGAS5005 Δ*sse* than that of wild-type
243 control mice (7, 31). PAF is an important lipid mediator in inflammation and chemoattractant
244 for neutrophils (35, 36). Deletion of *sse* leads to the reduction of the capacity of MGAS315 to
245 inhibit neutrophil recruitment inside GAS sites, suggesting that PAF may play a critical role in
246 neutrophils recruitment in the presence of SLS. Whether PAF mainly functions as
247 chemoattractant for neutrophils in GAS infections is currently investigated in our laboratory.
248 The difference in transepithelial migration of neutrophils between the treatments of the HaCaT
249 human keratinocyte cells with wild-type and SLS-negative GAS mutant suggests that SLS
250 inhibits the host cells' production of signals chemotactic for neutrophils (28). SLS can promotes
251 programmed cell death of epithelial keratinocytes during GAS infection (37). In the MGAS315
252 Δ*sse* infections, necrotic cells were present at the edge of bacteria sites on day 1 and inside GAS
253 sites on day 2 after inoculation, suggesting that SLS may kill neutrophils when they encounter
254 GAS bacteria and affect neutrophil recruitment at early stage of infection and result in the
255 histological pattern of Δ*sse* infection at day 1 after inoculation.

256 There is a synergistic effect of *sse* and *sagA* deletions on GAS loads in the liver and
257 spleen in subcutaneous infection of mice. The *sse* and *sagA* deletion mutants were not efficiently
258 cleared at skin infection sites, and the growth factors of the mutants in nonimmune human blood
259 and serum are similar to those of the parent strain. These observations suggest that Sse and SLS
260 synergistically contribute to GAS dissemination and systemic infections by hypervirulent GAS.

MATERIALS AND METHODS

Declaration of ethical approval. All animal procedures were carried out in strict accordance with the recommendations in the Guide for the Care and Use of Laboratory Animals of the National Institutes of Health (38). The protocols for the experiments were approved by the Institutional Animal Care and Use Committee at Montana State University (Permit number: 2014-45). Blood was collected from healthy donors in accordance with a protocol approved by the Institutional Review Board at MSU (Protocol No.: BL120513). Written informed consent was provided by study participants.

Bacterial strains and growth. Genotype *emm*3 strain MGAS315 has been described (29), and this hypervirulent clinical isolate has function-losing CovS G457V mutation (30). MGAS315 and its derivative strains were grown in Todd-Hewitt broth supplemented with 0.2% yeast extract (THY).

Generation of MGAS315 Δ*sse*, Δ*sagA*, and Δ*sse*Δ*sagA* mutants. MGAS315 Δ*sse* was generated using the suicide plasmid pGRV-Δ*sse* (16), as described (16). The mutant lacked a 621-bp fragment that encodes amino acids 55 to 261 of Sse and had no foreign DNA including antibiotic selection marker.

In the deletion of the *sagA* gene, a DNA fragment containing the whole *sagA* gene and its 23-bp upstream and 164-bp downstream was deleted whereas the downstream *sagB* was intact. The 5′and 3′ ~1,000-bp flanking fragments of the *sagA* fragment to be deleted were amplified from MGAS315 chromosomal DNA and using high fidelity Phusion DNA polymerase and primer pairs 5’-AGATCTGCAAACGTGTTCAATTGGTTG-3’/5’-CTCGAGTAACTGATAAGAACACGAG-3’ and 5’-

TTCTCGAGCTAGATAGTACCTGCTAATTAC-3'/5'-TTGGATCCGAAATGTCACGACACGAAC-3'. The PCR products of the upstream and downstream flanking fragments were sequentially cloned into pGRV (39) at the BglII/XhoI and XhoI/BamHI sites, respectively, yielding the suicide plasmid pGRV-Δ*sagA*. The plasmid was introduced into MGAS315 using electroporation and inserted into the *sagA* locus of the MGAS315 chromosome through a homologous recombination event at one flanking fragment. Bacteria with this first crossover were selected on THY agar plates with 10 mg/l chloramphenicol. One strain with the first crossover was grown on THY agar plate. At every 12 h after plating, bacteria were recovered from a whole plate, resuspended in 10 ml THY, and vortexed for 2 min, and 10 μl of the vortexed GAS suspension was streaked on THY agar plate, which was regarded as one passage. Deletion mutants were identified after >12 passages. Bacteria were plated on THY agar plates after the last passage, and resultant colonies were spotted in parallel on THY agar with and without chloramphenicol to identify potential double-crossover strains that were chloramphenicol-sensitive. Chloramphenicol-sensitive strains were analyzed to identify deletion mutants by PCR using primers 5'-GTGATAAGAACTAGATAGTTG-3' and 5'-GGCATTAAATGTTGAGCAAC-3'. The *sagA* gene in MGAS315 Δ*sse* was deleted similarly to yield Δ*sse*Δ*sagA*.

The *sse* and *sagA* deletions in the mutants were confirmed by DNA sequencing of the *sse* and *sagA* loci and by the loss of the Sse activity in culture supernatant of Δ*sse* mutants using the PAF acetylhydrolase activity assay (31) and by the loss of β-hemolytic activity of Δ*sagA* mutants on blood agar plates.

Construction of complement strains. The *sse* gene was put back into Δ*sse* and Δ*sse*Δ*sagA* using pGRV-*sse* (16), as previously described (16), yielding Δ*sse*-*sse* and

307 Δ*sse*Δ*sagA-sse* for complementation of the *sse* deletion mutants. For the complementation of the
308 *sagA* deletion mutants in Δ*sagA* and Δ*sse*Δ*sagA*, a fragment containing the full-length *sagA* gene
309 and its flanking regions was amplified with PCR using the Phusion High Fidelity PCR kit from
310 New England BioLabs, MGAS315 genomic DNA, and primers 5'-
311 TTGGATCCGCAAACGTGTTCAATTGGTTG-3' and 5'-
312 TTGGATCCGAAATGTCACGACACGAAC-3'. The PCR product was cloned into pGRV at
313 *Bam*HI site, yielding suicide plasmid pGRV-*sagA*. This plasmid was introduced into Δ*sagA* and
314 Δ*sse*Δ*sagA* by electroporation. The procedures described above to generate the Δ*sagA* mutant
315 were followed to generate complement strains Δ*sagA-sagA* and Δ*sse*Δ*sagA-sagA*. These
316 complement strains were confirmed by sequencing the *sse* or *sagA* loci. The Δ*sse-sse* and
317 Δ*sse*Δ*sagA-sse* strains restored production of Sse as assayed for the Sse enzymatic activity in its
318 culture supernatant using the Sse PAF acetylhydrolase activity assay (31), and the Δ*sagA-sagA*
319 and Δ*sse*Δ*sagA-sagA* strains restored SLS production as the strains displayed β-hemolytic
320 activity on blood agar plates.

321 **Subcutaneous Mouse infections.** Six-week old, female CD-1 and female and male
322 C57BL/6J mice were used in subcutaneous infections with MGAS315, Δ*sse*, Δ*sagA*, Δ*sse*Δ*sagA*,
323 and complement strains of the mutants. CD-1 mice were purchased from Charles River
324 Laboratories, and C57BL/6J mice were breed at the Animal Resources Center at Montana State
325 University using the breeding mice from The Jackson Laboratory. GAS bacteria grown in THY
326 were harvested at the exponential growth phase and washed with pyrogen-free Dulbecco's
327 phosphate-buffered saline (DPBS) three times, and resuspended in DPBS. Groups of mice were
328 subcutaneously inoculated with 0.2 ml of GAS in DPBS at OD_{600} of 1.0, and actual inoculum
329 was determined by plating and usually contained about 10^8 colony-forming units (cfu). Mice

were euthanized at indicated time after inoculation to collect skin samples for measurement of lesion size, viable bacteria, and neutrophil recruitment and histological analyses, and the liver and spleen were also harvested to measure numbers of viable GAS. The euthanasia of mice was done with a gradual fill method at a displacement rate of 30% CO_2 of the chamber volume per minute, as recommended in The 2013 American Veterinary Medical Association Guidelines.

Measurement of skin lesion size, neutrophil recruitment, and viable GAS in tissues. The skin around the infection site was peeled off, and the skin lesion was recognized by the boundary of the inflammation area. The size of skin lesions was measured by analyzing the lesion pictures using the area measurement tool of the Adobe Acrobat 9 software program. The skin containing infection area was excised for neutrophil measurement. Numbers of recruited neutrophils in the infected skin samples were determined by a myeloperoxidase assay, as described previously (7). The numbers of viable GAS in skin infection sites, liver and spleen were determined by homogenizing the tissues in DPBS using Kontes pestles and then plating at appropriate dilutions.

Histological analyses. Skin GAS infection sites collected at 24 h and 48 h after inoculation were fixed in 10% neutral buffered formalin for 24 h. The samples were dehydrated with ethanol, cleared with xylene, and infiltrated with paraffin using a Tissue Embedding Console System (Sakura Finetek, Inc.). The paraffin blocks were processed to obtain 4-μm sections, which were stained with hematoxylin and eosin (H&E) or with a Gram stain kit from Becton, Dickinson and Company. Stained slides were examined using a Nikon Eclipse 80i microscope.

GAS growth in nonimmune human blood and pooled mouse blood. GAS growth in nonimmune blood and serum from two persons and pooled blood of female C57BL/6J mice was

353 determined as previously described (7). Bacteria of MGAS315, Δ*sse*, Δ*sagA*, Δ*sse*Δ*sagA*, and
354 complement strains were harvested at the exponential growth phase in THY, washed three times
355 with DPBS, and inoculated in triplicates at ~ 10^5 CFU/ml into 0.5 ml of heparinized nonimmune
356 human blood or serum and into 0.2 ml of heparinized mouse blood pool. The samples were
357 rotated end-to-end for 3 h at 37°C, and the numbers of viable GAS in the samples and inocula
358 were determined by plating. The growth factor was defined as the ratio of CFU for each sample
359 after a 3-h incubation over the CFU of the corresponding inoculum.

360 **Other analyses.** DNA sequencing of the amplified PCR products was performed by
361 using the BigDye Terminator v3.1 cycle sequencing kit and an Applied Biosystems 3130 genetic
362 analyzer. Sequence data were analyzed by using Sequencer 5.1 software (Gene Codes
363 Corporation). The PAF acetylhydrolase activity in culture supernatant of MGAS315 and its
364 isogenic mutants was assayed using the 2-thio PAF-based colorimetric assay as described (31).

365 **Statistical analyses**. The statistical analyses were done using the GraphPad Prism
366 software (version 7.03). The data of lesion size, neutrophil recruitment, GAS loads in mouse
367 infections were analyzed by the Mann-Whitney *t* Test, and the growth factors in human blood
368 and serum and mouse blood were analyzed by the 1 way ANOVA multiple comparison analyses.
369

370 **ACKNOWLEDGEMENTS**

371 This work was supported in part by grants AI095704, AI097703, and GM110732 from the
372 National Institutes of Health, Montana University System Research Initiative 51040-
373 MUSRI2015-03, and the Montana State Agricultural Experimental Station.
374

REFERENCES

1. **Carapetis JR, Steer AC, Mulholland EK, Weber M.** 2005. The global burden of group A streptococcal diseases. Lancet Infect Dis **5**:685–694.
2. **Nelson GE, Pondo T, Toews KA, Farley MM, Lindegren ML, Lynfield R, Aragon D, Zansky SM, Watt JP, Cieslak PR, Angeles K, Harrison LH, Petit S, Beall B, Van Beneden CA**. 2016. Epidemiology of invasive group A streptococcal infections in the United States, 2005-2012. Clin Infect Dis **63:**478-486.
3. **Sharkawy A, Low DE, Saginur R, Gregson D, Schwartz B, Jessamine P, Green K, McGeer A; Ontario Group A Streptococcal Study Group**. 2002. Severe group a streptococcal soft-tissue infections in Ontario: 1992-1996. Clin Infect Dis **34**:454-460.
4. **Olsen RJ, Musser JM**. 2010. Molecular pathogenesis of necrotizing fasciitis. Annu Rev Pathol **5**:1–31.
5. **Dahl PR, Perniciaro C, Holmkvist KA, O'Connor MI, Gibson LE.** 2002. Fulminant group A streptococcal necrotizing fasciitis: clinical and pathologic findings in 7 patients. J Am Acad Dermatol **47**:489-492.
6. **Bakleh M, Wold LE, Mandrekar JN, Harmsen WS, Dimashkieh HH, Baddour LM.** 2005. Correlation of histopathologic findings with clinical outcome in necrotizing fasciitis. Clin Infect Dis **40**:410-414.
7. **Liu M, Zhu H, Li J, Garcia CC, Feng W, Kirpotina LN, Hilmer J, Tavares LP, Layton AW, Quinn MT, Bothner B, Teixeira MM, Lei B.** 2012. Group A *Streptococcus* secreted esterase hydrolyzes platelet-activating factor to impede neutrophil recruitment and facilitate innate immune evasion. PLoS Pathog **8:**e1002624.
8. **Li J, Zhu H, Feng W, Liu M, Song Y, Zhang X, Zhou Y, Bei W, Lei B.** 2013. Regulation

of inhibition of neutrophil infiltration by the two-component regulatory system CovRS in subcutaneous murine infection with group A *Streptococcus*. Infect Immun **81:**974-983.

9. **Miyoshi-Akiyama T, Ikebe T, Watanabe H, Uchiyama T, Kirikae T, Kawamura Y.** 2006. Use of DNA arrays to identify a mutation in the negative regulator, csrR, responsible for the high virulence of a naturally occurring type M3 group A streptococcus clinical isolate. J Infect Dis **193**:1677-1684.
10. **Sumby P, Whitney AR, Graviss EA, DeLeo FR, Musser JM.** 2006. Genome-wide analysis of group A streptococci reveals a mutation that modulates global phenotype and disease specificity. PLoS Pathog **2:**41-49.
11. **Levin JC, Wessels MR.** 1998. Identification of *csrR/csrS*, a genetic locus that regulates hyaluronic acid capsule synthesis in group A *Streptococcus*. Mol Microbiol **30:**209-219.
12. **Heath A, DiRita VJ, Barg NL, Engleberg NC.** 1999. A two-component regulatory system, CsrR-CsrS, represses expression of three *Streptococcus pyogenes* virulence factors, hyaluronic acid capsule, streptolysin S, and pyrogenic exotoxin B. Infect Immun **67:**5298-5305.
13. **Federle MJ, McIver KS, Scott JR.** 1999. A response regulator that represses transcription of several virulence operons in the group A *Streptococcus*. J Bacteriol **181:**3649-3657.
14. **Treviño J, Perez N, Ramirez-Peña E, Liu Z, Shelburne SA 3rd, Musser JM, Sumby P.** 2009. CovS simultaneously activates and inhibits the CovR-mediated repression of distinct subsets of group A *Streptococcus* virulence factor-encoding genes. Infect Immun **77:**3141-3149.
15. **Edwards RJ, Taylor GW, Ferguson M, Murray S, Rendell N, Wrigley A, Bai Z, Boyle J, Finney SJ, Jones A, Russell HH, Turner C, Cohen J, Faulkner L, Sriskandan S.** 2005.

421 Specific C-terminal cleavage and inactivation of interleukin-8 by invasive disease isolates of
422 *Streptococcus pyogenes*. J Infect Dis **192:**783-790.
423 **16. Zhu H, Liu M, Sumby P, Lei B.** 2009. The secreted esterase of group a streptococcus is
424 important for invasive skin infection and dissemination in mice. Infect Immun **77:**5225-5232.
425 **17. Lei B**, **DeLeo FR, Hoe NP, Graham MR, Mackie SM, Cole RL, Liu M, Hill HR, Low**
426 **DE, Federle MJ, Scott JR, Musser JM**. 2001. Evasion of human innate and acquired
427 immunity by a bacterial homolog of CD11b that inhibits opsonophagocytosis. Nat Med
428 **7**:1298-1305.
429 **18. Bricker AL, Carey VJ, Wessels MR**. 2005. Role of NADase in virulence in experimental
430 invasive group A streptococcal infection. Infect Immun **73:**6562-6566.
431 **19. O'Seaghdha M, Wessels MR**. 2013. Streptolysin O and its co-toxin NAD-glycohydrolase
432 protect group A *Streptococcus* from xenophagic killing. PLoS Pathog **9:**e1003394.
433 **20. Walker MJ, Hollands A, Sanderson-Smith ML, Cole JN, Kirk JK, Henningham A,**
434 **McArthur JD, Dinkla K, Aziz RK, Kansal RG, Simpson AJ, Buchanan JT, Chhatwal**
435 **GS, Kotb M, Nizet V.** 2007. DNase Sda1 provides selection pressure for a switch to
436 invasive group A streptococcal infection. Nat Med **13**:981-985.
437 **21. Kansal RG, Datta V, Aziz RK, Abdeltawab NF, Rowe S, Kotb M.** 2010. Dissection of the
438 molecular basis for hypervirulence of an in vivo-selected phenotype of the widely
439 disseminated M1T1 strain of group A Streptococcus bacteria. J Infect Dis **201**:855-865.
440 **22. Engleberg NC, Heath A, Miller A, Rivera C, DiRita VJ.** 2001. Spontaneous mutations in
441 the CsrRS two-component regulatory system of *Streptococcus pyogenes* result in enhanced
442 virulence in a murine model of skin and soft tissue infection. J Infect Dis **183:**1043-1054.

443 **23. Cole JN, Pence MA, von Köckritz-Blickwede M, Hollands A, Gallo RL, Walker MJ,**
444 **Nizet V.** 2010. M protein and hyaluronic acid capsule are essential for *in vivo* selection of
445 *covRS* mutations characteristic of invasive serotype M1T1 group A *Streptococcus*. MBio
446 **1**:e00191-10.
447 **24. Liu G, Feng W, Li D, Liu M, Nelson DC, Lei B.** 2015. The Mga Regulon but Not
448 Deoxyribonuclease Sda1 of invasive M1T1 group A *Streptococcus* contributes to *in vivo*
449 selection of CovRS mutations and resistance to innate immune killing mechanisms. Infect
450 Immun **83:**4293-4303.
451 **25. Feng W, Liu M, Chen DG, Yiu R, Fang FC, Lei B.** 2016. Contemporary pharyngeal and
452 invasive *emm*1 and invasive *emm*12 group A *Streptococcus* isolates exhibit similar *in vivo*
453 selection for CovRS mutants in mice. PLoS One **11:**e0162742.
454 **26. Feng W, Minor D, Liu M, Li J, Ishaq SL, Yeoman C, Lei B**. 2017. Null Mutations of
455 Group A Streptococcus Orphan Kinase RocA: Selection in Mouse Infection and Comparison
456 with CovS Mutations in Alteration of In Vitro and In Vivo Protease SpeB Expression and
457 Virulence. Infect Immun **85(1)**:e00790-16.
458 **27. Li J, Liu G, Feng W, Zhou Y, Liu M, Wiley JA, Lei B**. 2014. Neutrophils select
459 hypervirulent CovRS mutants of M1T1 group A *Streptococcus* during subcutaneous infection
460 of mice. Infect Immun **82:**1579-1590.
461 **28. Lin A, Loughman JA, Zinselmeyer BH, Miller MJ, Caparon MG.** 2009. Streptolysin S
462 inhibits neutrophil recruitment during the early stages of Streptococcus pyogenes infection.
463 Infect Immun **77**:5190-5201.
464 **29. Beres SB, Sylva GL, Barbian KD, Lei B, Hoff JS, Mammarella ND, Liu MY, Smoot JC,**
465 **Porcella SF, Parkins LD, Campbell DS, Smith TM, McCormick JK, Leung DY,**

Schlievert PM, Musser JM. 2002. Genome sequence of a serotype M3 strain of group A Streptococcus: phage-encoded toxins, the high-virulence phenotype, and clone emergence. Proc Natl Acad Sci USA **99**:10078-10083.

30. **Stetzner ZW, Li D, Feng W, Liu M, Liu G, Wiley J, Lei B**. 2015. Serotype M3 and M28 Group A Streptococci Have Distinct Capacities to Evade Neutrophil and TNF-α Responses and to Invade Soft Tissues. PLoS One 10:e0129417.
31. **Liu G**, **Liu M, Xie G, Lei B**. 2013. Characterization of streptococcal platelet-activating factor acetylhydrolase variants that are involved in innate immune evasion. Infect Immun **81**:3128-3138.
32. **Liu M, Feng W, Zhu H, Lei B**. 2015. A Neutralizing Monoclonal IgG1 Antibody of Platelet-Activating Factor Acetylhydrolase SsE Protects Mice against Lethal Subcutaneous Group A Streptococcus Infection. Infect Immun **83**:2796-2805.
33. **Nizet V, Beall B, Bast DJ, Datta V, Kilburn L, Low DE, De Azavedo JC.** 2000. Genetic locus for streptolysin S production by group A streptococcus. Infect Immun **68**:4245-4254.
34. **Datta V, Myskowski SM, Kwinn LA, Chiem DN, Varki N, Kansal RG, Kotb M, Nizet V.** 2005. Mutational analysis of the group A streptococcal operon encoding streptolysin S and its virulence role in invasive infection. Mol Microbiol **56**:681-695.
35. **Venable ME, Zimmerman GA, McIntyre TM, Prescott SM**. 1993. Platelet-activating factor: a phospholipid autacoid with diverse actions. J Lipid Res **34**:691-702.
36. **Shaw JO, Pinckard RN, Ferrigni KS, McManus LM, Hanahan DJ**. 1981. Activation of human neutrophils with 1-O-hexadecyl/octadecyl-2-acetyl-sn-glycerol-3-phosphorylcholine (platelet activating factor). J Immunol **127**:1250-1255.

488 **37. Flaherty RA, Puricelli JM, Higashi DL, Park CJ, Lee SW.** 2015. Streptolysin S Promotes
489 Programmed Cell Death and Enhances Inflammatory Signaling in Epithelial Keratinocytes
490 during Group A Streptococcus Infection. Infect Immun **83**:4118-4133.
491 **38. National Research Council**. Guide for the care and use of laboratory animals, 8th ed.
492 National Academies Press, Washington, DC. 2011.
493 **39. Liu M, Hanks TS, Zhang J, McClure MJ, Siemsen DW, Elser JL, Quinn MT, Lei B**. 2006.
494 Defects in ex vivo and in vivo growth and sensitivity to osmotic stress of group A *Streptococcus*
495 caused by interruption of response regulator gene vicR. Microbiology **152**:967-978.
496
497
498 **(FIGURE LEGENDS)**
499 **FIG. 1. Effects of *sse* and *sagA* deletions on skin invasion, GAS loads in liver and spleen,**
500 **and neutrophil recruitment in subcutaneous MGAS315 infection of CD-1 mice.** Six-week
501 old female CD-1 mice were subcutaneously inoculated with 1.7 x 10^8 CFU MGAS315, 2.0 x10^8
502 cfu Δ*sse*, 2.1 x 10^8 cfu Δ*sagA*, and 1.7 x 10^8 cfu Δ*sse*Δ*sagA* and euthanized at 48 h after
503 inoculation for analyses. Shown are representative inside-out images of the skin infection sites
504 (A), lesion size (B), neutrophil recruitment (C), GAS loads in spleen (D), and GAS load in liver
505 (E). The Mann-Whitney *t* Test: *, $P < 0.05$; **, $P < 0.01$; and ***, $P < 0.001$.

506 **FIG. 2. Effects of *sse* and *sagA* deletions on skin invasion, GAS loads in liver and spleen,**
507 **and neutrophil recruitment in subcutaneous MGAS315 infection of C57BL/6J mice.** six-
508 week old C57BL/6J mice were subcutaneously inoculated with 1.5 x 10^8 CFU MGAS315, 1.9
509 x10^8 cfu Δ*sse*, 1.8 x 10^8 cfu Δ*sagA*, and 1.7 x 10^8 cfu Δ*sse*Δ*sagA* and euthanized at 24 h after
510 inoculation for analyses. Shown are lesion size (A), neutrophil recruitment (B), GAS loads in

liver (C), and GAS load in spleen (D). The Mann-Whitney *t* Test: *, $P < 0.05$; **, $P < 0.01$; ***, $P < 0.001$; ****, and $P < 0.0001$.

FIG. 3. Lack of the detrimental effect of *sse* and *sagA* deletion on the clearance of MGAS315 at skin infection sites and human blood. (A) Persistence of MGAS315, Δ*sse*, Δ*sagA*, Δ*sse*Δ*sagA* at skin infection sites. About 10^8 cfu bacteria of each strain were subcutaneously inoculated in groups of sixteen 6-week old female C57BL/6J mice. Eight mice of each group were euthanized at 1 h and 24 h after inoculation. Presented are the numbers and median values of viable GAS at the skin infection sites. The P values are for 1 h versus 24 h comparison of each strain by the Mann-Whitney *t* Test. (B) Growth factors of MGAS315 and its derivative strains in nonimmune blood and serum. The strains were inoculated ($\sim 10^5$ CFU) into 0.5 ml of nonimmune blood or serum in triplicates and incubated for 3 h at 37°C with end-to-end rotation. Growth factor was defined as the ratio of viable CFU of GAS in each sample over the CFU of the inoculum. The 1way ANOVA multiple comparison analyses: $P \geq 0.1184$.

FIG. 4. **Histological analyses of MGAS315, Δ*sse*, Δ*sagA*, and Δ*sse*Δ*sagA* skin infection sites in mice at day 1 after inoculation**. Groups of ten 6-week old female C57BL/6J mice were subcutaneously inoculated with 1.5×10^8 cfu MGAS315, 1.8×10^8 cfu Δ*sse*, 1.9×10^8 cfu Δ*sagA*, 2.0×10^8 cfu Δ*sse*Δ*sagA* in 0.2 ml DPBS. Five mice of each group were sacrificed on days 1 and 2 after inoculation, respectively, to collect skin infection sites. The skin infection sites were fixed and analyzed with Gram and H&E stains, as described in the Materials and Methods section. Shown are representative Gram and H&E stain images of infection sites. Shown are the Gram and H&E stain images for the regions in skin infection site that are indicated by the boxes in Figs. S1, S3, S5, and S7. The bar represents 20 μm.

FIG. 5. **Histological analyses of MGAS315, Δ*sse*, Δ*sagA*, and Δ*sse*Δ*sagA* skin infection sites in mice at day 2 after inoculation**. The infection conditions were described in Fig. 4. Shown are representative Gram and H&E stain images of infection sites. Shown are the Gram and H&E stain images for the regions in skin infection site that are indicated by the boxes in Figs. S2, S4, S6, and S8. The bar represents 20 μm.

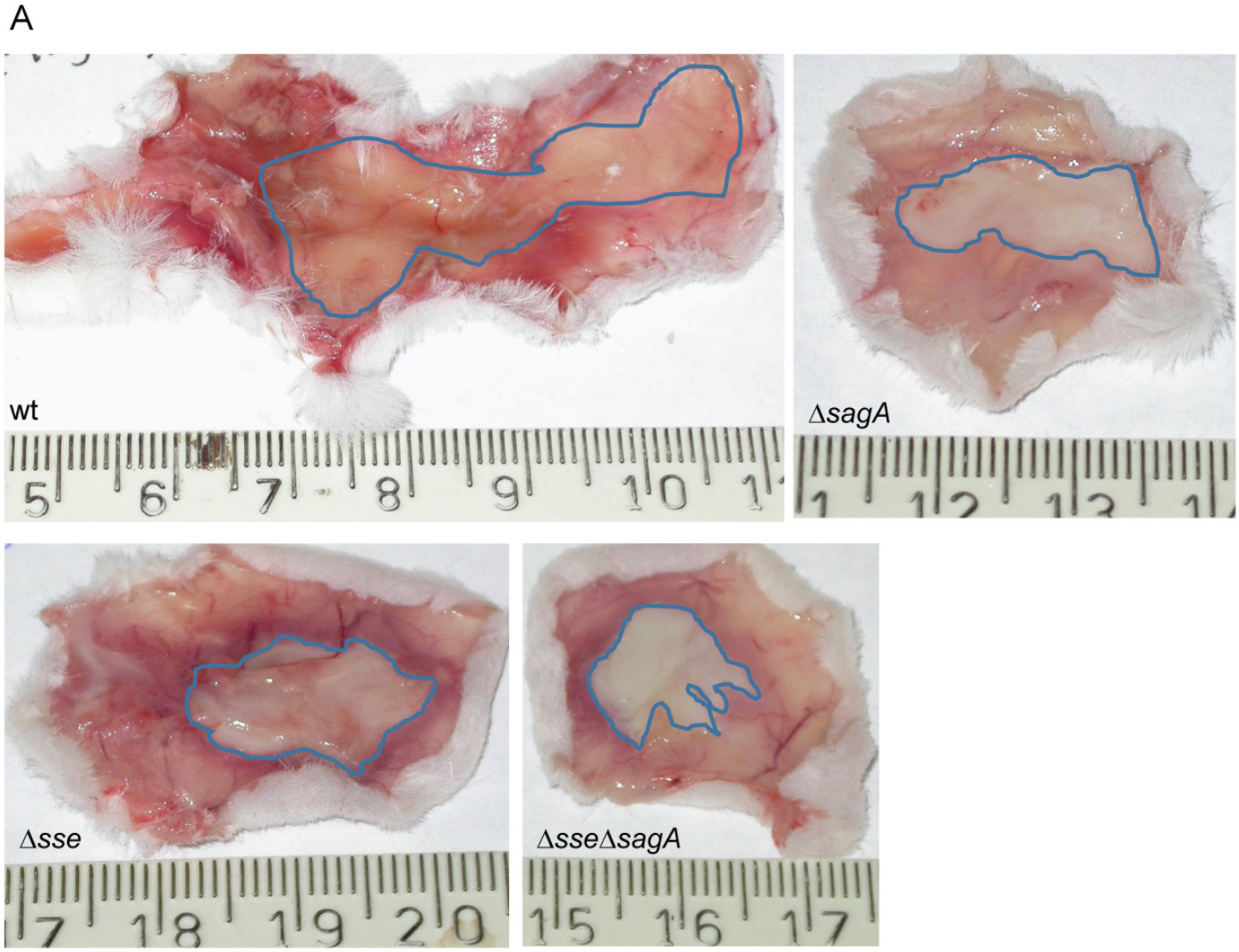
A
wt
ΔsagA
Δsse
ΔsseΔsagA

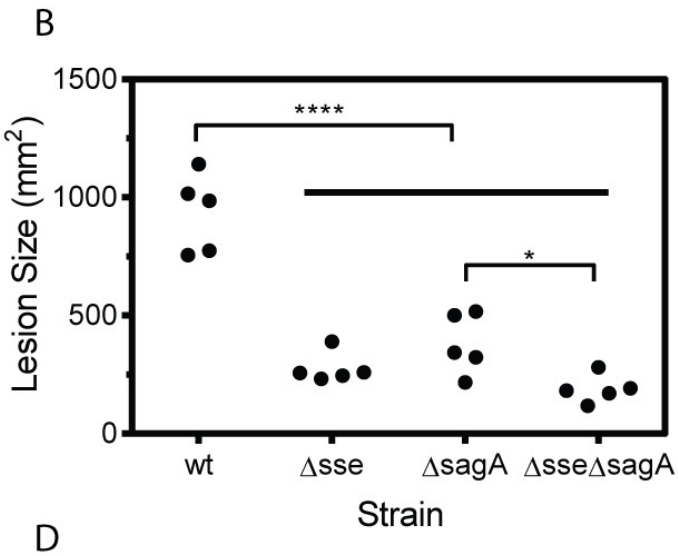
B
Lesion Size (mm²)
1500
1000
500
0
****
*
wt
Δsse
ΔsagA
ΔsseΔsagA
Strain

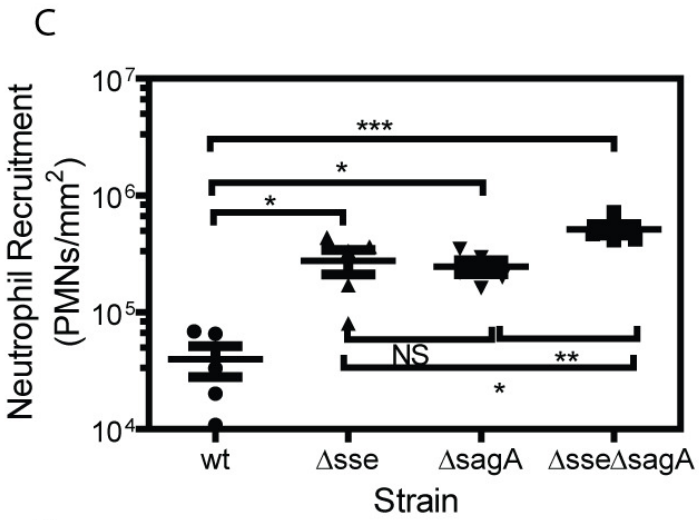
C
Neutrophil Recruitment (PMNs/mm²)
10⁷
10⁶
10⁵
10⁴
***
*
*
NS
**
*
wt
Δsse
ΔsagA
ΔsseΔsagA
Strain

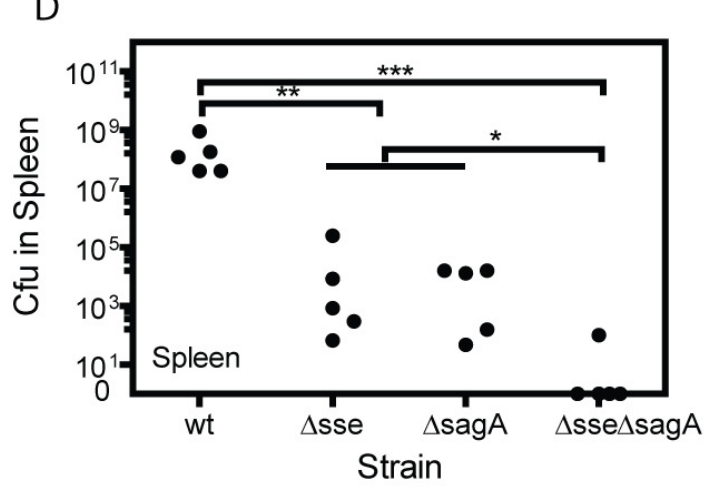
D
Cfu in Spleen
10¹¹
10⁹
10⁷
10⁵
10³
10¹
0
***
**
*
Spleen
wt
Δsse
ΔsagA
ΔsseΔsagA
Strain

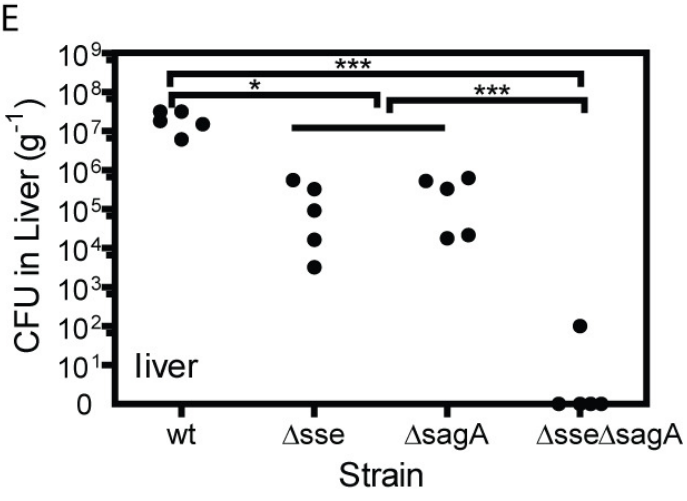
E
CFU in Liver (g⁻¹)
10⁹
10⁸
10⁷
10⁶
10⁵
10⁴
10³
10²
10¹
0
***
*
***
liver
wt
Δsse
ΔsagA
ΔsseΔsagA
Strain

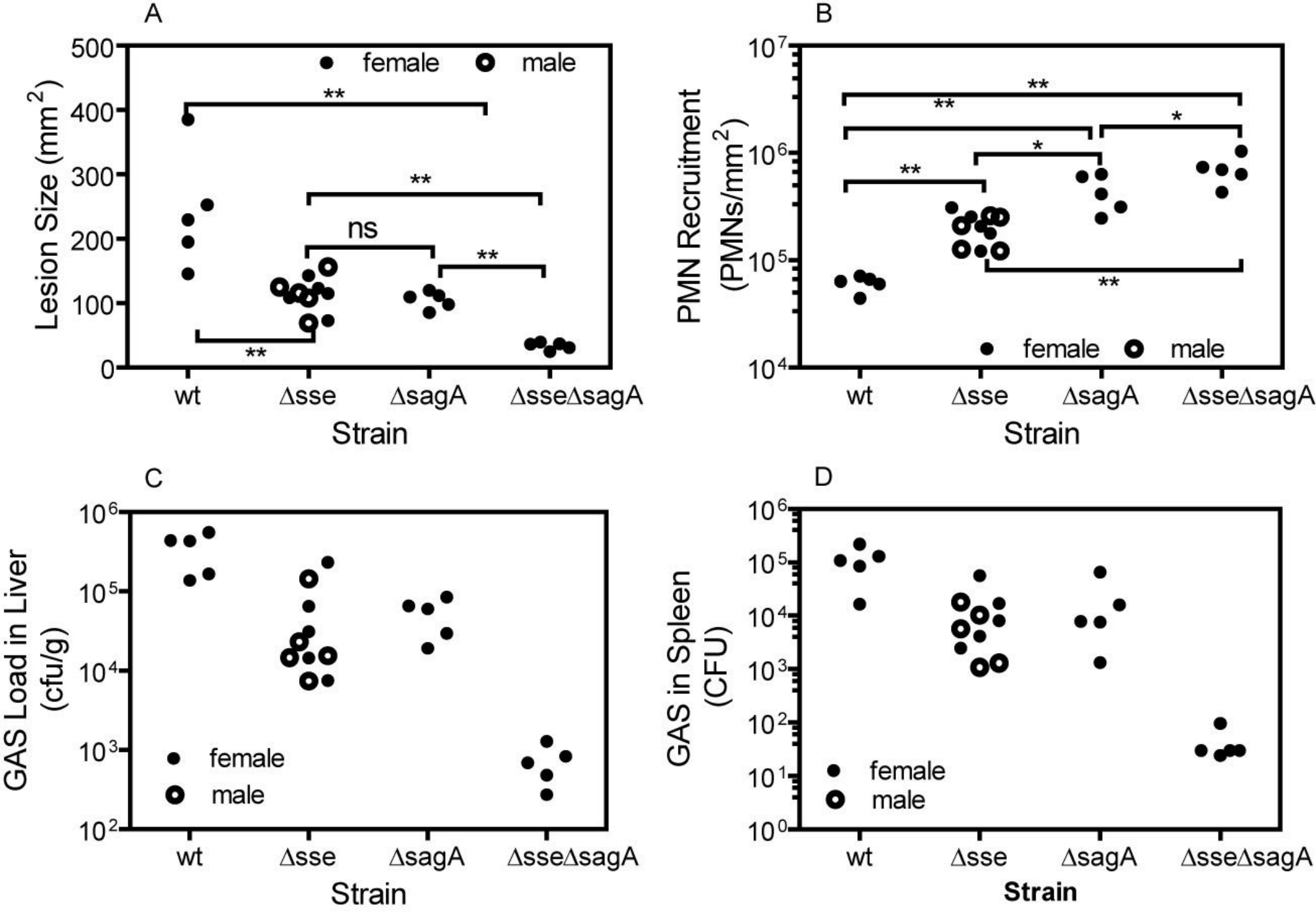
A
Lesion Size (mm^2)
500
400
300
200
100
0
female
male
**
**
ns
**
**
wt
Δsse
ΔsagA
ΔsseΔsagA
Strain
B
PMN Recruitment (PMNs/mm^2)
10^7
10^6
10^5
10^4
**
**
*
*
**
female
male
wt
Δsse
ΔsagA
ΔsseΔsagA
Strain
C
GAS Load in Liver (cfu/g)
10^6
10^5
10^4
10^3
10^2
female
male
wt
Δsse
ΔsagA
ΔsseΔsagA
Strain
D
GAS in Spleen (CFU)
10^6
10^5
10^4
10^3
10^2
10^1
10^0
female
male
wt
Δsse
ΔsagA
ΔsseΔsagA
Strain

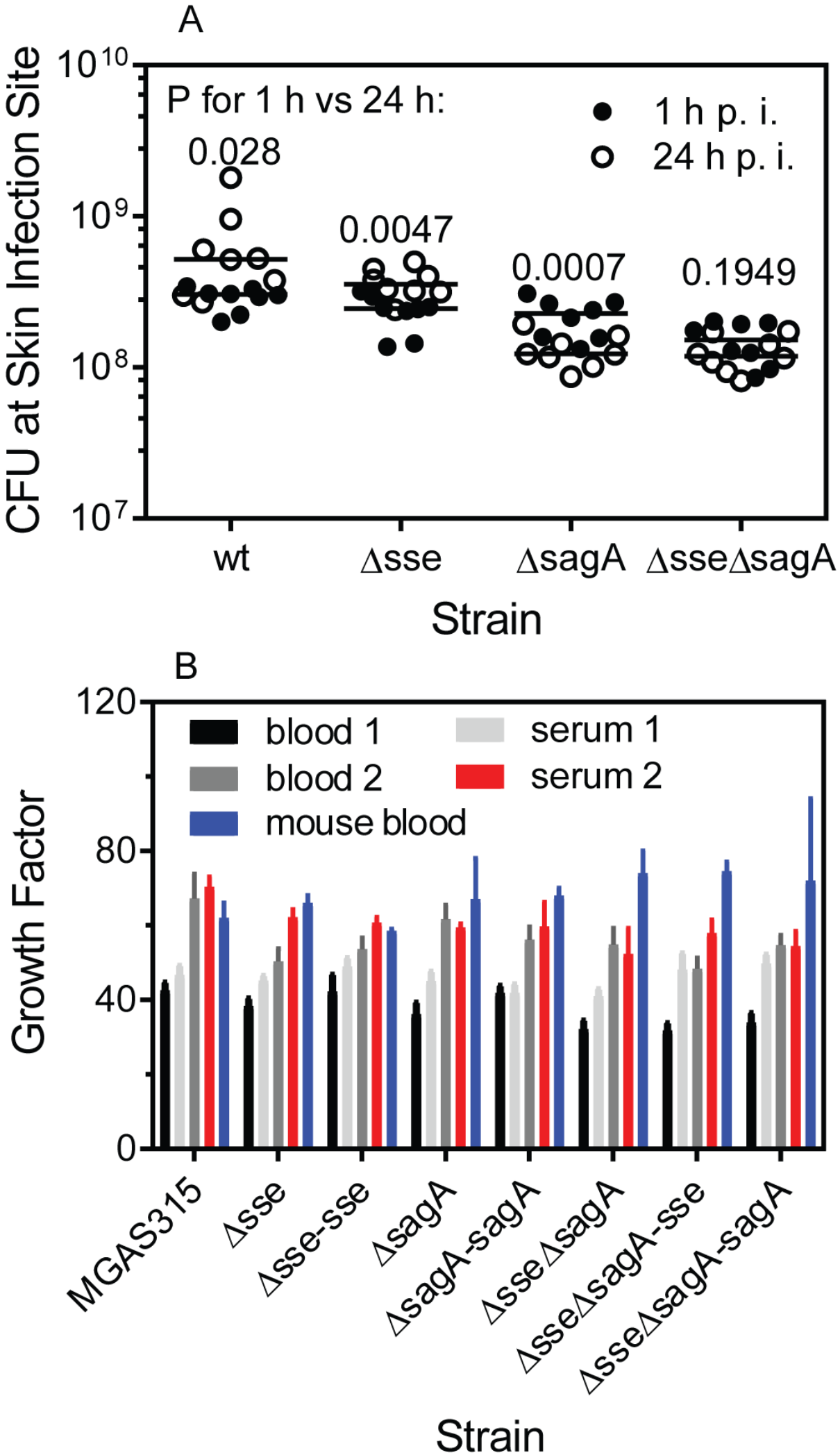
A
CFU at Skin Infection Site
10^{10}
10^{9}
10^{8}
10^{7}
P for 1 h vs 24 h:
0.028
0.0047
0.0007
0.1949
1 h p. i.
24 h p. i.
wt
Δsse
ΔsagA
ΔsseΔsagA
Strain
B
Growth Factor
120
80
40
0
blood 1
blood 2
mouse blood
serum 1
serum 2
MGAS315
Δsse
Δsse-sse
ΔsagA
ΔsagA-sagA
ΔsseΔsagA
ΔsseΔsagA-sse
ΔsseΔsagA-sagA
Strain

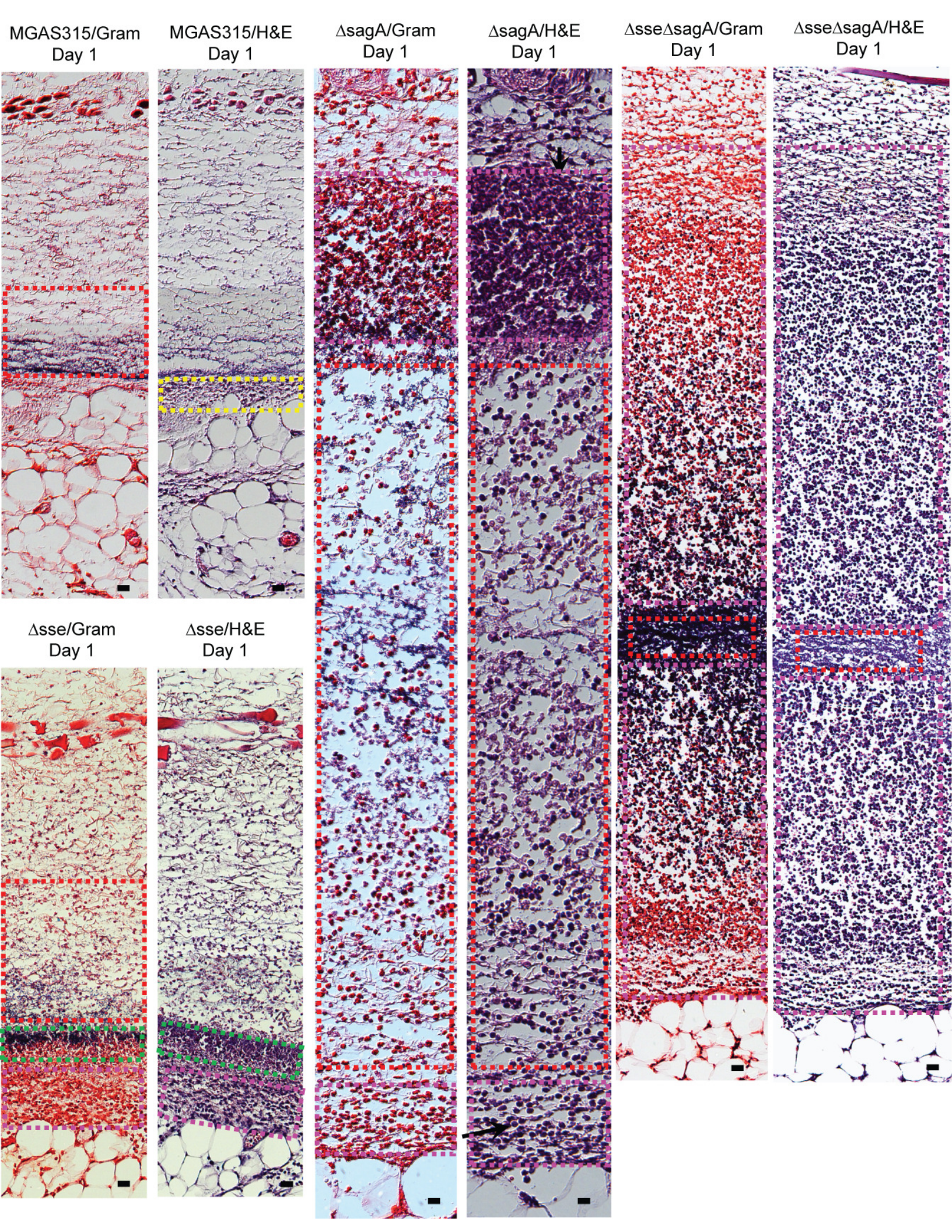
MGAS315/Gram
Day 1
MGAS315/H&E
Day 1
ΔsagA/Gram
Day 1
ΔsagA/H&E
Day 1
ΔsseΔsagA/Gram
Day 1
ΔsseΔsagA/H&E
Day 1
Δsse/Gram
Day 1
Δsse/H&E
Day 1

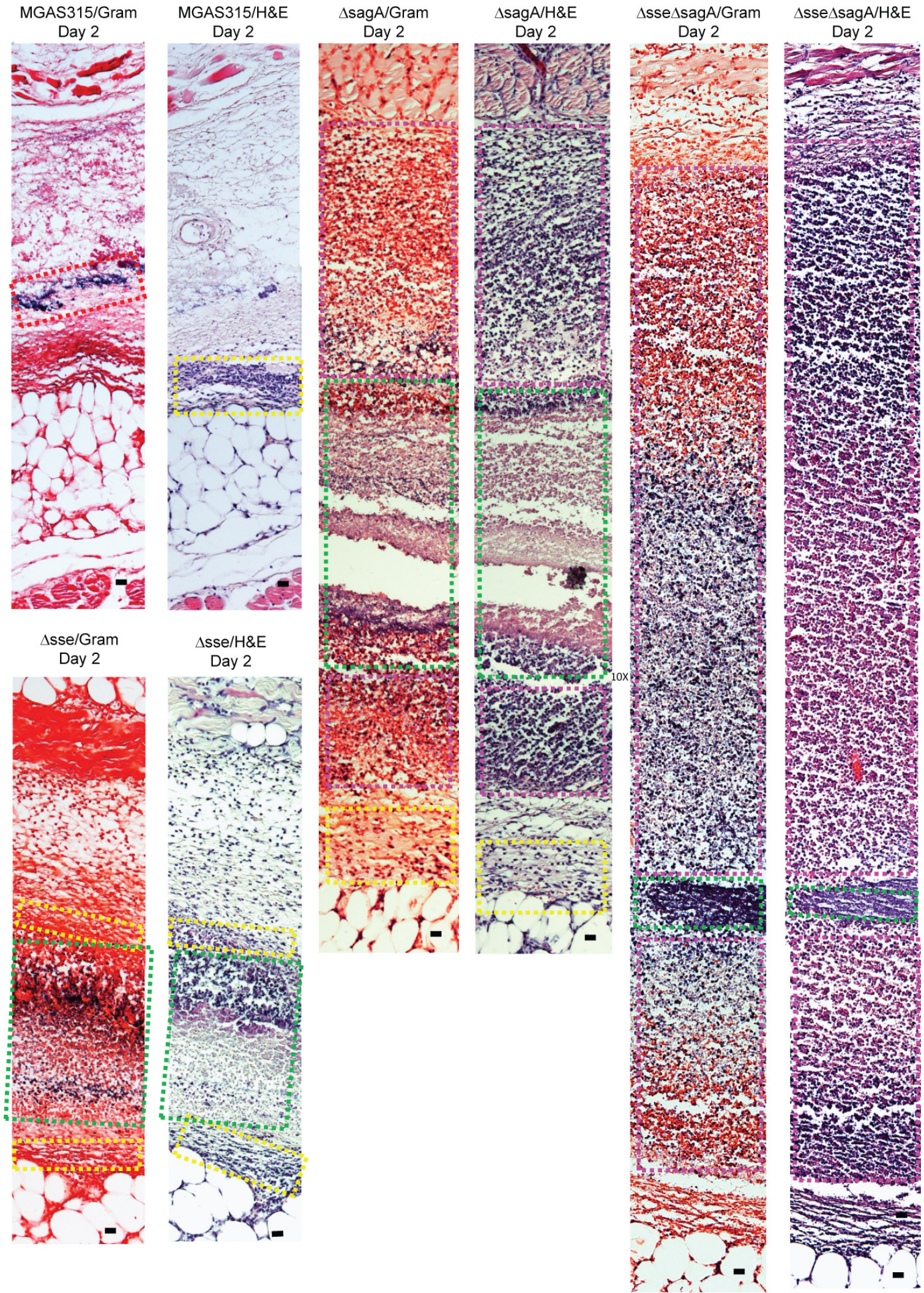
MGAS315/Gram
Day 2
MGAS315/H&E
Day 2
ΔsagA/Gram
Day 2
ΔsagA/H&E
Day 2
ΔsseΔsagA/Gram
Day 2
ΔsseΔsagA/H&E
Day 2
Δsse/Gram
Day 2
Δsse/H&E
Day 2
10X